Focussed on "Crack Paths"

Visual Abstract

Evaluation of fatigue properties under four-point bending and fatigue crack propagation in austenitic stainless steel with a bimodal harmonic structure

Shoichi Kikuchi
Shizuoka University, Japan
kikuchi.shoichi@shizuoka.ac.jp, http://orcid.org/0000-0003-1127-8748

Yuta Nakatsuka, Yoshikazu Nakai
Kobe University, Japan
161t347t@stu.kobe-u.ac.jp
nakai@mech.kobe-u.ac.jp, http://orcid.org/0000-0002-4146-6670

Masashi. Natakani, Mie. Ota. Kawabata, Kei. Ameyama
Ritsumeikan University, Japan
rm005034@ed.ritsumei.ac.jp
mie-ota@fc.ritsumei.ac.jp, https://orcid.org/0000-0002-3991-274X
ameyama@se.ritsumei.ac.jp, https://orcid.org/0000-0002-4479-854X

ABSTRACT. Austenitic stainless steel (JIS-SUS304L) with a bimodal harmonic structure, which is defined as a coarse-grained structure surrounded by a network of fine grains, was fabricated using powder metallurgy to improve both the strength and ductility. Four-point bending fatigue tests and *K*-decreasing tests were conducted in air at room temperature under a stress ratio *R* of 0.1 to investigate fatigue crack propagation in SUS304L. The fatigue limit of this harmonic-structured material is higher than that of the material with a homogeneous coarse-grained structure. This is attributable to the formation of fine grains by mechanical milling and to the suppression of pore formation. In contrast, the threshold stress intensity range, ΔK_{th}, for the harmonic-structured material is lower than that for the homogeneous coarse-grained material, while the crack growth rates, da/dN, are higher at comparable ΔK. These results can be attributed to a reduction in the effective threshold stress intensity range, $\Delta K_{eff,th}$, due to the presence of fine grains in the harmonic structure.

KEYWORDS. Fatigue; Fracture mechanics; Crack closure; Grain refinement; Powder metallurgy; Stainless steel.

OPEN ACCESS

Citation: Kikuchi, S., Nakatsuka, Y., Nakai, Y., Nakatani, M., Kawabata, M.O., Ameyama, K., Evaluation of Fatigue Properties under Four-point Bending and Fatigue Crack Propagation in Austenitic Stainless Steel with a Bimodal Harmonic Structure, Frattura ed Integrità Strutturale, 48 (2019) 545-553.

Received: 12.11.2018
Accepted: 22.12.2018
Published: 01.04.2019

Copyright: © 2019 This is an open access article under the terms of the CC-BY 4.0, which permits unrestricted use, distribution, and reproduction in any medium, provided the original author and source are credited.

INTRODUCTION

Austenitic stainless steel has been widely used in various engineering fields because of its high heat resistance, high corrosion resistance, and excellent formability [1]. Recent years have seen a rise in the demand for improvement in the mechanical properties of structural steels, including the present austenitic stainless steel. Thus, increasing the structural reliability of steels has become important. The microstructures and mechanical properties of stainless steels can be controlled by surface modification [2-7], the addition of different alloying elements [7, 8], and grain refinement [2, 5, 9, 10]. Grain refinement through severe plastic deformation is particularly effective in strengthening metallic materials; however, it leads to a decrease in ductility [9, 11, 12].

In order to suppress the decrease in ductility due to the formation of a homogeneous fine-grained structure, new microstructural designs were proposed [11-17]. Our research group has designed a harmonic structure using powder metallurgy to sinter mechanically milled stainless steel powders [18-23], which improve both their strength and ductility by suppressing necking during tensile deformation [20]. In particular, we have focused on the fatigue properties under four-point bending [24-27] and near-threshold fatigue propagation of long cracks [28-30] in titanium-based materials with a bimodal harmonic structure. To achieve sufficient performance with the newly developed harmonic structured stainless steels, their fatigue properties and fatigue crack propagation behavior need to be examined.

The purpose of the present study is to elucidate the mechanism of fatigue fracture in bimodal harmonic-structured austenitic stainless steel under four-point bending, and to examine the effects of the bimodal harmonic structure on the fatigue crack propagation in austenitic stainless steel.

EXPERIMENTAL PROCEDURES

Material and specimens

This study employed austenitic stainless steel (JIS-SUS304L) containing 19.35% Cr, 9.18% Ni, 1.83% Mn, 0.25% Si, and 0.02% C (all by mass, with the balance being Fe). This material was made into a powder (particle diameter: 120 μm) through a plasma rotating electrode process that can be used to fabricate spherical particles with negligible contamination by impurities such as oxygen or nitrogen gas [31].

A bimodal microstructural design using mechanical milling (MM) and spark plasma sintering (SPS) was introduced for the formation of the harmonic-structured SUS304L. MM was performed for 180 ks in Ar at room temperature for the SUS304L powders using a planetary ball mill (Fritch P-5) with a tungsten carbide vessel and steel ball bearings to form fine grains on the particle surfaces. The rotation speed was 200 rpm, and the ball-to-powder mass ratio was 2:1. The powders were subsequently consolidated by SPS at 1223 K for 3.6 ks under vacuum (less than 15 Pa) and applied pressure (50 MPa) using a 25-mm internal diameter graphite die to produce the specimens, hereafter referred to as the "MM series." A second set of specimens was prepared by sintering the as-received powders (hereafter, the "untreated series") for comparison. The tensile strength of the MM series was higher than that of the untreated series, but the elongations of the two series were almost the same [19, 20]. The MM series has a Vickers hardness of 169.6±2.5 HV, as measured for a polished surface with an indentation force of 1.961 N and a load holding time of 10 s (n = 30). Hardness value of the MM series is higher than that of the untreated series (125.2±3.6 HV).

The sintered materials were sliced into disks approximately 1.5 mm thick and machined into a blunt-notched specimen for four-point bending fatigue tests [26, 27]. After machining, the specimen surface was polished with emery paper (#240 to #4000) to a thickness of 1 mm and polished in a SiO_2 suspension to obtain a mirror finish. The notch roots of the specimen were also polished with emery paper (#240) to remove the electro-discharge machined layer.

Testing

Four-point bending fatigue tests were performed in an electrodynamic fatigue testing system under a stress ratio R of 0.1. The frequency of stress cycling was 10 Hz, and the tests were conducted in ambient conditions. Fatigue tests were interrupted after a certain number of cycles, and acetyl cellulose films were placed on the specimen surface using the replica method to examine fatigue crack initiation and propagation. Once the crack length was measured using optical microscopy, the stress intensity range, ΔK, was calculated [27, 28, 32]; the aspect ratio, c/a, for small cracks was estimated as follows:

$$c/a = 1 - 1.607(a/t) + 1.080(a/t)^2 - 0.2149(a/t)^3 \quad \text{for } a/t < 1 \text{ and} \tag{1}$$

$$c/a = 0.259 \quad \text{for } a/t > 1, \tag{2}$$

where a is the crack length on the surface, c is the crack length along the thickness direction, and t is the specimen thickness. K-decreasing tests were also conducted to approach the fatigue threshold. The present study employed disk-shaped compact (DC(T)) specimens (2 mm thick) [28-30] in accordance with the ASTM standard. The tests were conducted in the ambient laboratory atmosphere under a stress ratio R of 0.1. The fatigue threshold, ΔK_{th}, is defined as the maximum value of ΔK under a crack growth rate of 10^{-10} m/cycle. Crack lengths were monitored by the unloading elastic compliance method [33]. The magnitude of crack closure was also monitored; the closure stress intensity, K_{cl}, was obtained from the closure load, P_{cl}. After the fatigue tests, fracture surfaces and crack profiles were observed using scanning electron microscopy (SEM), and the microstructure around the crack paths was analyzed using electron backscattered diffraction (EBSD) at an acceleration voltage of 20 kV.

RESULTS AND DISCUSSION

Microstructural characterization

The microstructure of sintered compacts was characterized using EBSD. The image quality (IQ) map and grain boundary map obtained by EBSD analysis for the MM series is shown in Fig. 1. In the present study, the grain boundary is defined as the high-angle grain boundaries greater than 15°. The MM series contained regions of fine equiaxed grains and regions with a coarse microstructure. The regions of fine equiaxed grains formed a continuous connected three-dimensional network that surrounded the coarse-grained structure. This network is referred to as a harmonic structure in the present study.

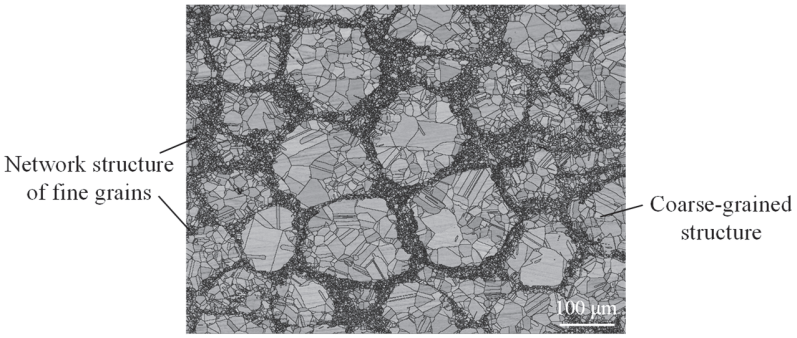

Figure 1: Image quality (IQ) map and grain boundary map obtained by EBSD analysis for MM series.

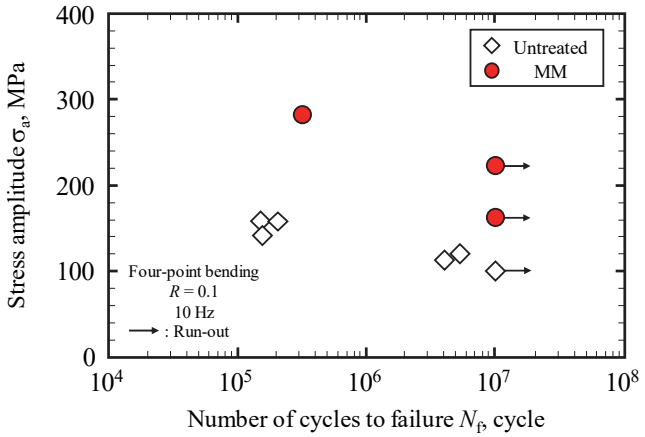

Figure 2: Results of four-point bending fatigue tests, showing stress amplitude as a function of cycles to failure.

Fatigue properties determined by four-point bending

Fig. 2 shows the results of four-point bending fatigue tests for the sintered compacts (untreated and MM series); a stress amplitude, σ_a, was applied to the specimen surface as a function of the number of cycles to failure, N_f. In this figure, those plots with an arrow represent the run-out specimens without failure at $N = 10^7$ cycles. The fatigue limit, which was defined as the average value of the maximum stress amplitude without fatigue failure and the minimum stress amplitude with fatigue

failure, for the MM series (260 MPa) with high hardness was higher than that for the untreated series (105 MPa). Sufficient data could not be obtained for the MM series because some MM series specimens did not exhibit fatigue failure at stress amplitudes above 280 MPa owing to plastic deformation.

Fig. 3 shows SEM fractographs of the MM series (N_f = 3.4×10^5 cycles), which failed at σ_a = 280 MPa, and of the untreated series (N_f = 5.6×10^6 cycles), which failed at σ_a = 120 MPa. In all micrographs, the surface subjected to tensile stress is the upper surface. Macroscopic observation revealed only one fatigue crack near the specimen surface, which gradually propagated across the cross-section of the specimen. The fracture surface of the MM series specimen is divided into two regions by a clear boundary, as is shown in Fig. 3(a). In contrast, a characteristic, powder-like microstructure is observed on the surface of the untreated series specimen (see Fig. 3(b)). These results indicate that the MM suppresses the formation of pores in SUS304L during the subsequent SPS process owing to plastic deformation [34] of the SUS304L powder surface. The formation of pores tends to be suppressed with increasing SPS temperature [35]; thus, the SPS temperature (1223 K) is not high enough for the initial SUS304L powder in the present study.

To elucidate the mechanism of fatigue crack initiation in the harmonic-structured SUS304L, EBSD analysis was conducted on the specimens after fatigue testing. Figs. 4 shows the inverse pole figure (IPF) map obtained by EBSD for the fracture surface near the crack initiation site of the MM series and a schematic in which the red square indicates the analyzed region in the MM series. A fatigue crack was initiated in the coarse-grained (> 10 μm) structure of the harmonic-structured MM series. In addition, the fatigue crack profile is not influenced by the harmonic structure, and propagates perpendicular to the loading direction. These same effects have also been observed with a Ti-6Al-4V alloy [24, 25] and CP titanium [27].

Furthermore, Zhang et al. [23] reported that the fatigue limit for the harmonic-structured JIS-SUS316L austenitic stainless steel tends to increase as the MM time increases under uniaxial stress loading, because the areal fraction of the fine-grained structure tends to increase as the MM time increases [25, 36]. The harmonic structure increases the fatigue limit of SUS304 owing to grain refinement and the suppression of pore formation during the SPS process.

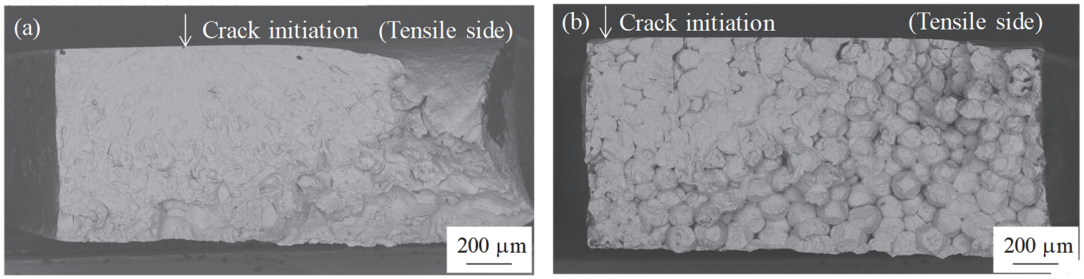

Figure 3: SEM fractographs of the (a) MM series (N_f = 3.4x10^5 cycles) failed at σ_a = 280 MPa and (b) untreated series (N_f = 5.6x10^6 cycles) failed at σ_a = 120 MPa.

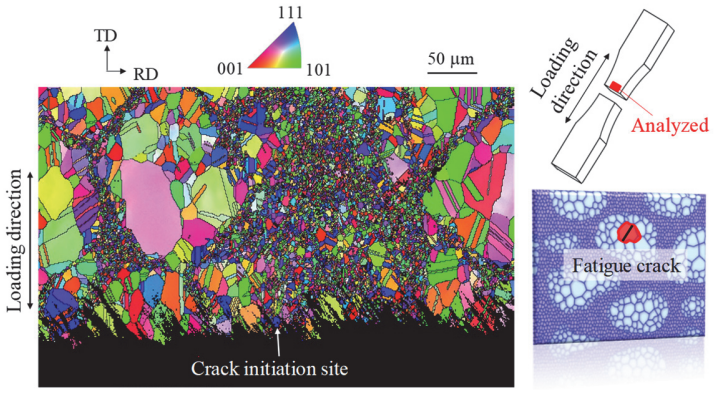

Figure 4: Inverse pole figure (IPF) map obtained by EBSD analysis for MM series that failed at a stress amplitude of 280 MPa (N_f = 3.4×10^5 cycles).

Fatigue crack propagation behavior

To examine the effect of pores on the fatigue properties of SUS304L, small fatigue crack propagation was examined by the replica method for the untreated series with pores. In the present study, small fatigue crack propagation in the MM series is not examined because the MM series have no pores. Fig. 5 shows optical micrographs of the surface of the untreated series

tested at σ_a = 160 MPa and observed after a given number of loading cycles. Fig. 5 reveals that a 17-μm-long fatigue crack was initiated from a pore after 8.5×10⁴ cycles (Fig. 5(b)). Subsequently, multiple cracks were initiated from pores and gradually propagated (Figs. 5(c)-(g)). Fatigue cracks, which were initiated from pores, coalesced at several instants and the final fracture occurred at 2.08×10⁵ cycles.

Fig. 6(a) plots the crack growth rate, da/dN, of long cracks for the untreated and MM series against ΔK. In both series, da/dN decreases with decreasing ΔK and the da/dN values for the MM series are consistently higher than those for the untreated specimens at comparable ΔK levels. Furthermore, the ΔK_{th} value for the untreated series is higher than that for the MM series. The long fatigue crack growth resistance of SUS304L is reduced owing to the presence of the harmonic structure.

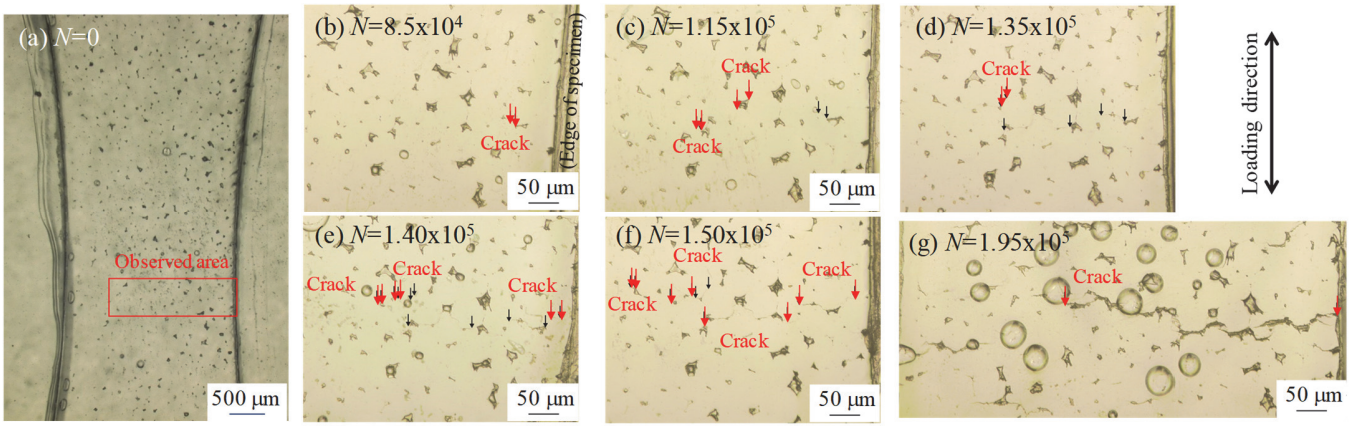

Figure 5: Optical fractographs of untreated series that failed at a stress amplitude of 160 MPa (N_f = 2.08×10⁵ cycles).

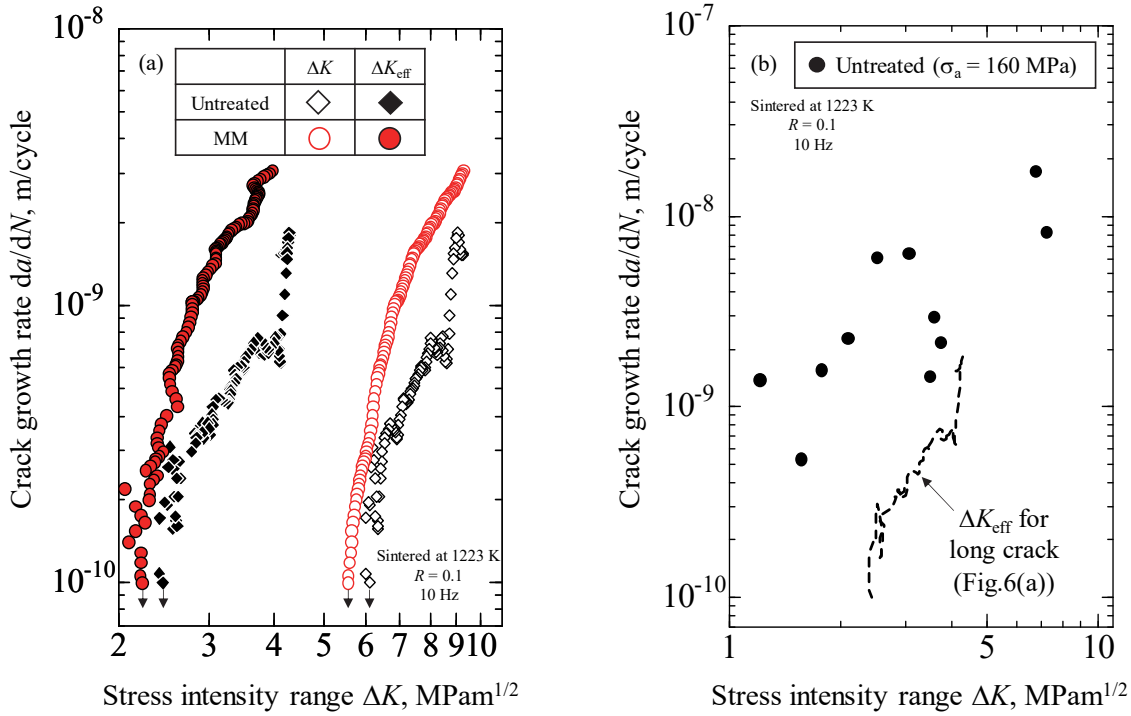

Figure 6: Relationship between (a) crack growth rate and stress intensity range for the untreated series and MM series, and (b) crack growth rate and stress intensity range for the untreated series with a long crack and a small crack.

Furthermore, the da/dN against ΔK_{eff} for the untreated and MM series are also plotted in Fig. 6(a), which reveals that the $\Delta K_{eff,th}$ value for the untreated series is higher than that for the MM series. This indicates that the effect of the harmonic

structure at near-threshold levels is attributable not to crack closure but to grain size, i.e., the effect of slip-band growth resistance by grain boundaries and misorientations [37, 38]. This same effect, in which a bimodal harmonic structure affects $\Delta K_{eff,th}$, has also been observed for a Ti-6Al-4V alloy [29].

To compare the small and long crack propagation behaviors of SUS304L, the crack growth rate, da/dN, under four-point bending is calculated using the data shown in Fig. 5. Fig. 6(b) plots the dependence of the crack growth rate, da/dN, on ΔK for small and long cracks in the untreated series. For the small crack, the da/dN values are slightly higher than those for the long crack under comparable ΔK. In addition, a small crack in the untreated series propagates at ΔK values lower than the $\Delta K_{eff,th}$ for a long crack. The results show that the ΔK_{th} value for small cracks in the untreated series is lower than that for long cracks with the elimination of crack closure. The same effect has been observed for metallic materials [39, 40]. Consequently, the harmonic-structured SUS304L exhibits a lower resistance to fatigue crack growth owing to grain refinement, and the formation of pores is suppressed by MM. In the future, the three-dimensional fatigue crack shape [41-46] and the misorientations near the crack initiation site [47-49] will be measured for SUS304L with fatigue damage using synchrotron radiation to describe the mechanism of fatigue crack initiation and propagation in greater detail.

Conclusions

The effect of a bimodal harmonic structure on the fatigue properties under four-point bending and fatigue crack propagation in austenitic stainless steel (JIS-SUS304L) was investigated. The main conclusions obtained can be summarized as follows:

(1) Mechanical milling suppresses the formation of pores in SUS304L during the subsequent sintering process, owing to the plastic deformation of SUS304L powder surface.

(2) The harmonic-structured SUS304L exhibits a higher fatigue limit than the sintered compact prepared from as-received powders, which had pores and a coarse microstructure.

(3) The da/dN values for harmonic-structured SUS304L are higher than those for steel fabricated from as-received powders with coarse grains for comparable values of ΔK.

(4) The ΔK_{th} for harmonic-structured SUS304L is lower than that for steel fabricated from coarse-grained as-received powders. This difference is attributable to a reduction in $\Delta K_{eff,th}$, resulting from the presence of fine grains in the harmonic structure.

Acknowledgement

This work was supported by JSPS KAKENHI Grant Number JP15K05677 and JP18H05256.

References

[1] Baddoo, N.R. (2008). Stainless steel in construction: A review of research, applications, challenges and opportunities, J. Constr. Steel Res., 64(11), pp. 1199-1206. DOI: 10.1016/j.jcsr.2008.07.011.

[2] Kikuchi, S., Sasago, A., Komotori, J. (2009). Effect of simultaneous surface modification process on wear resistance of martensitic stainless steel, J. Mater. Process. Technol., 209(20), pp. 6156-6160. DOI: 10.1016/j.jmatprotec.2009.04.024

[3] Kikuchi, S., Nakahara, Y., Komotori, J. (2010). Fatigue properties of gas nitrided austenitic stainless steel pre-treated with fine particle peening, Int. J. Fatigue, 32(2), pp. 403-410. DOI: 10.1016/j.ijfatigue.2009.07.019.

[4] Kikuchi, S., Nakahara, Y., Dobashi, K., Komotori, J. (2012). Effects of FPP/gas nitriding hybrid surface treatment on fatigue properties of austenitic stainless steel (SUS316), J. Soc. Mater. Sci., Jpn., 61(8), pp. 680-685. DOI: 10.2472/jsms.61.680.

[5] Kikuchi, S., Yasutake, Y., Komotori, J. (2012). Effect of fine particle peening on oxidation resistance of austenitic stainless steel, J. Solid Mech. Mater. Eng., 6(6), pp. 431-439. DOI: 10.1299/jmmp.6.431.

[6] Kurashina, Y., Hamano, T., Miyata, S., Komotori, J., Koyama, T. (2014). Proliferation of calf chondrocyte on stainless-steel surfaces with different microtopography, J. Jpn. Inst. Met. Mater., 78(4), pp. 170-176.

DOI: 10.2320/jinstmet.J2013070.
[7] Kikuchi, S., Iwamae, S., Akebono, H., Komotori, J., Kadota, K. (2018). Effect of atmospheric-controlled induction-heating fine particle peening on electrochemical characteristics of austenitic stainless steel, Surf. Coat. Technol., 334, pp. 189-195. DOI: 10.1016/j.surfcoat.2017.08.001.
[8] Lewis, A.C., Bingert, J.F., Rowenhorst, D.J., Gupta, A., Geltmacher, A.B., Spanos, G. (2006). Two- and three-dimensional microstructural characterization of a super-austenitic stainless steel, Mater. Sci. Eng. A, 418(1-2), pp. 11-18. DOI: 10.1016/j.msea.2005.09.088.
[9] Chen, X.H., Lu, J., Lu, L., Lu, K. (2005). Tensile properties of a nanocrystalline 316L austenitic stainless steel, Scripta Mater., 52(10), pp. 1039-1044. DOI: 10.1016/j.scriptamat.2005.01.023.
[10] Schino, A.D., Kenny, J.M. (2003). Grain refinement strengthening of a micro-crystalline high nitrogen austenitic stainless steel, Mater. Lett., 57(12), pp. 1830-1834. DOI: 10.1016/S0167-577X(02)01076-5.
[11] Terada, D., Inoue S., Tsuji N. (2007). Microstructure and mechanical properties of commercial purity titanium severely deformed by ARB process, J. Mater. Sci., 42(5), pp. 1673-1681. DOI: 10.1007/s10853-006-0909-7.
[12] Terada, D., Inoue, M., Kitahara H., Tsuji N. (2008). Change in mechanical properties and microstructure of ARB processed Ti during annealing, Mater. Trans., 49(1), pp. 41-46. DOI: 10.2320/matertrans.ME200710.
[13] Wang, Y., Chen, M., Zhou, F., Ma, E. (2002). High tensile ductility in a nanostructured metal, Nature, 419, pp. 912–915. DOI: 10.1038/nature01133.
[14] Fang, T.H., Li, W.L., Tao, N.R., Lu, K. (2011). Revealing extraordinary intrinsic tensile plasticity in gradient nano-grained copper, Science, 331, pp. 1587–1590. DOI: 10.1126/science.1200177.
[15] Szabó, P.J., Field, D.P., Jóni, B, Horky, J., Ungár, T. (2015). Bimodal grain size distribution enhances strength and ductility simultaneously in a low-carbon low-alloy steel, Metall. Mat. Trans. A, 46(5), pp. 1948-1957. DOI: 10.1007/s11661-015-2783-x.
[16] Mimoto, T., Umeda, J., Kondoh, K. (2015). Titanium powders via gas-solid direct reaction process and mechanical properties of their extruded materials, Mater. Trans., 56(8), pp. 1153-1158. DOI: 10.2320/matertrans.L-M2015816.
[17] Mukai, T., Kawazoe, M., Higashi, K. (1998). Dynamic mechanical properties of a near-nano aluminum alloy processed by equal-channel-angular-extrusion, Nanostruct. Mater., 10(5), pp. 755-765. DOI: 10.1016/S0965-9773(98)00113-5.
[18] Ueno, A., Fujiwara, H., Rifai, M., Zhang, Z., Ameyama, K. (2012). Fractographical analysis on fracture mechanism of stainless steel having harmonic microstructure, J. Soc. Mater. Sci., Jpn., 61(8), pp. 686–691. DOI: 10.2472/jsms.61.686.
[19] Zhang, Z., Vajpai, S.K., Orlov, D., Ameyama, K. (2014). Improvement of mechanical properties in SUS304L steel through the control of bimodal microstructure characteristics, Mater. Sci. Eng. A, 598, pp. 106-113. DOI: 10.1016/j.msea.2014.01.023.
[20] Zhang, Z., Orlov, D., Vajpai, S.K., Tong, B., Ameyama, K. (2015). Importance of bimodal structure topology in the control of mechanical properties of a stainless steel, Adv. Eng. Mater., 17(6), pp. 791-795. DOI: 10.1002/adem.201400358.
[21] Rai, P.K., Shekhar, S., Nakatani, M., Ota, M., Vajpai, S.K., Ameyama, K., Mondal, K. (2017). Wear behavior of harmonic structured 304L stainless steel, J. Mater. Eng. Perform., 26(6), pp. 2608-2618. DOI: 10.1007/s11665-017-2719-2.
[22] Park, H.K., Ameyama, K., Yoo, J., Hwang, H., Kim, H.S. (2018). Additional hardening in harmonic structured materials by strain partitioning and back stress, Mater. Res. Lett., 6(5), pp. 261-267. DOI: 10.1080/21663831.2018.1439115.
[23] Zhang, Z., Ma, H., Zheng, R., Hu, Q., Nakatani, M., Ota, M., Chen, G., Chen, X., Ma, C., Ameyama, K. (2017). Fatigue behavior of a harmonic structure designed austenitic stainless steel under uniaxial stress loading, Mater. Sci. Eng. A, 707, pp. 287-294. DOI: 10.1016/j.msea.2017.09.063.
[24] Kikuchi, S., Takemura, K., Ueno, A., Ameyama, K. (2015). Evaluation of the 4-points bending fatigue properties of Ti-6Al-4V alloy with harmonic structure created by mechanical milling and spark plasma sintering, J. Soc. Mater. Sci. Jpn., 64(11), pp. 880-886. DOI: 10.2472/jsms.64.880.
[25] Kikuchi, S., Hayami, Y., Ishiguri, T., Guennec, B., Ota, M., Ueno, A., Ameyama, K. (2017). Effect of bimodal grain size distribution on fatigue properties of Ti-6Al-4V alloy with harmonic structure under four-point bending, Mater. Sci. Eng. A, 687, pp. 269-275. DOI: 10.1016/j.msea.2017.01.076.
[26] Kikuchi, S., Kubozono, H., Nukui, Y., Ueno, A., Kawabata, M.O., Ameyama, K. (2018). Statistical fatigue properties and small fatigue crack propagation in bimodal harmonic structured Ti-6Al-4V alloy under four-point bending, Mater. Sci. Eng. A, 711, pp. 29-36. DOI: 10.1016/j.msea.2017.11.010.
[27] Nukui, Y., Kubozono, H., Kikuchi, S., Nakai, Y., Ueno, A., Kawabata, M.O., Ameyama, K. (2018). Fractographic analysis of fatigue crack initiation and propagation in CP titanium with a bimodal harmonic structure, Mater. Sci. Eng. A, 716, pp. 228-234. DOI: 10.1016/j.msea.2018.01.054.

[28] Kikuchi, S., Imai, T., Kubozono, H., Nakai, Y., Ueno, A., Ameyama, K. (2015). Evaluation of near-threshold fatigue crack propagation in Ti-6Al-4V alloy with harmonic structure created by mechanical milling and spark plasma sintering, Frattura ed Integrità Strutturale, 34(9), pp. 261-270. DOI: 10.3221/IGF-ESIS.34.28.
[29] Kikuchi, S., Imai, T., Kubozono, H., Nakai, Y., Ota, M., Ueno, A., Ameyama, K. (2016). Effect of harmonic structure design with bimodal grain size distribution on near-threshold fatigue crack propagation in Ti-6Al-4V Alloy, Int. J. Fatigue, 92(2), pp. 616-622. DOI: 10.1016/j.ijfatigue.2016.02.038.
[30] Kikuchi, S., Mori, T., Kubozono, H., Nakai, Y., Kawabata, M.O., Ameyama, K. (2017). Evaluation of near-threshold fatigue crack propagation in harmonic-structured CP Titanium with a bimodal grain size distribution, Eng. Fract. Mech., 181, pp. 77-86. DOI: 10.1016/j.engfracmech.2017.06.026.
[31] Tokizane, M., Isonishi, K. (1992). Production of uniformly-sized spherical powder by plasma rotating electrode process and its applications to some intermetallics powders, J. Jpn. Soc. Powder Metal., 39(12), pp. 1137-1144. DOI: 10.2497/jjspm.39.1137.
[32] Newman, J.C., Raju, I.S. (1984). Stress-intensity factor equations for cracks in three-dimensional finite bodies subjected to tension and bending loads, NASA Langley Res. Ctr., Hampton, VA(NASA Technical Memorandum 85793).
[33] Kikukawa, M., Jono, M., Tanaka, K., Takatani, M. (1976). Measurement of fatigue crack propagation and crack closure at low stress intensity level by unloading elastic compliance method, J. Soc. Mater. Sci., Jpn., 25(276), pp. 899-903. DOI: 10.2472/jsms.25.899.
[34] Ohsawa, H., Nishimura, H. (1989). Manufacturing methods of superplastic materials and commercial applications, J. Jpn Inst. Light Metals, 39(11), pp. 765-775. DOI: 10.2464/jilm.39.765.
[35] Kikuchi, S., Akebono, H., Ueno, A., Ameyama, K. (2018). Formation of commercially pure titanium with a bimodal nitrogen diffusion phase using plasma nitriding and spark plasma sintering, Powder Technol., 344, pp. 410-417. DOI: 10.1016/j.powtec.2018.02.047.
[36] Kikuchi, S., Nakamura, Y., Ueno, A., Ameyama, K. (2015). Low temperature nitriding of commercially pure titanium with harmonic structure, Mater. Trans., 56(11), pp. 1807-1813. DOI: 10.2320/matertrans.Y-M2015822.
[37] Taira, S., Tanaka, K., Nakai, Y. (1978). A model of crack-tip slip band blocked by grain boundary, Mech. Res. Comm., 5(6), pp. 375-381. DOI: 10.1016/0093-6413(78)90014-9.
[38] Shibanuma, K., Ueda, K., Ito, H., Nemoto, Y., Kinefuchi, M., Suzuki, K., Enoki, M. (2018). Model for predicting fatigue life and limit of steels based on micromechanics of small crack growth, Mater. Design, 139, pp. 269-282. DOI: 10.1016/j.matdes.2017.10.069 .
[39] Tanaka, K., Nakai, Y., Yamashita, M. (1981). Fatigue growth threshold of small cracks, Int. J. Fract., 17(5), pp. 519-533. DOI: 10.1007/BF00033345
[40] Suresh, S., Ritchie, R.O. (1984). Propagation of short fatigue cracks, Int. Metals Rev., 29(1), pp. 445–476. DOI: 10.1179/imtr.1984.29.1.445.
[41] Makino, T., Neishi, Y., Shiozawa, D., Kikuchi, S., Okada, S., Kajiwara K., Nakai, Y. (2015). Effect of defect length on rolling contact fatigue crack propagation in high strength steel, Frattura ed Integrita Strutturale, 34(9), pp. 334-340. DOI: 10.3221/IGF-ESIS.34.36.
[42] Nakai, Y., Shiozawa, D., Kikuchi, S., Sato, K., Obama, T. (2015). In situ observation of rolling contact fatigue cracks by laminography using ultrabright synchrotron radiation, Frattura ed Integrita Strutturale, 34(9), (2015) pp. 246-254. DOI: 10.3221/IGF-ESIS.34.26.
[43] Nakai, Y., Shiozawa, D., Kikuchi, S., Obama, T., Saito, H., Makino, T., Neishi, Y. (2016). Effects of inclusion size and orientation on rolling contact fatigue crack initiation observed by laminography using ultra-bright synchrotron radiation, Procedia Structural Integrity, 2, pp. 3117-3124. DOI: 10.1016/J.PROSTR.2016.06.389.
[44] Makino, T., Neishi, Y., Shiozawa, D., Kikuchi, S., Okada, S., Kajiwara K., Nakai, Y. (2016). Effect of defect shape on rolling contact fatigue crack initiation and propagation in high strength steel, Int. J. Fatigue, 92(2), pp. 507-516. DOI: 10.1016/j.ijfatigue.2016.02.015.
[45] Nakai, Y., Shiozawa, D., Kikuchi, S., Obama, T., Saito, H., Makino T., Neishi, Y. (2017). 4D observations of rolling contact fatigue processes by laminography using ultra-bright synchrotron radiation, Eng. Fract. Mech., 183, pp. 180-189. DOI: 10.1016/j.engfracmech.2017.03.021.
[46] Makino, T., Neishi, Y., Shiozawa, D., Kikuchi, S., Saito, H., Kajiwara K., Nakai, Y. (2017). Rolling contact fatigue damage from artificial defects and sulphide inclusions in high strength steel, Procedia Structural Integrity, 7, pp. 468-475. DOI: 10.1016/j.prostr.2017.11.114.
[47] Nakai, Y., Shiozawa, D., Nakao, R., Asakawa N., Kikuchi, S. (2016). Misorientation measurement of individual grains in fatigue of polycystalline alloys by diffraction contrast tomography using ultrabright synchrotron radiation, Mater. Sci. Forum, 879, pp. 1355-1360. DOI: 10.4028/www.scientific.net/MSF.879.1355.

[48] Nakai, Y., Shiozawa, D., Asakawa, N., Nonaka, K., Kikuchi, S. (2017). Change of misorientation of individual grains in fatigue of polycrystalline alloys by diffraction contrast tomography using ultrabright synchrotron radiation, Procedia Structural Integrity, 3, pp. 402-410. DOI: 10.1016/j.prostr.2017.04.058.

[49] Shiozawa, D., Nakai, Y., Miura, R., Masuda, N., Matsuda, S., Nakao, R. (2016). 4D evaluation of grain shape and fatigue damage of individual grains in polycrystalline alloys by diffraction contrast tomography using ultrabright synchrotron radiation, Int. J. Fatigue, 82(2), pp. 247-255. DOI: 10.1016/j.ijfatigue.2015.07.014.